Calibration methods for laser ablation Rb–Sr geochronology: comparisons and recommendation based on NIST glass and natural reference materials

Stijn Glorie[1*], Sarah E. Gilbert[2], Martin Hand[1], Jarred C. Lloyd[1]

[1] *Department of Earth Sciences, University of Adelaide, SA 5005, Australia.*

[2] *Adelaide Microscopy, University of Adelaide, SA 5005, Australia.*

Correspondence to: Stijn Glorie (stijn.glorie@adelaide.edu.au)

Abstract

In-situ Rb–Sr geochronology using LA-ICP-MS/MS technology allows rapid dating of K-rich minerals such as micas (e.g. biotite, muscovite, phlogopite) and K-feldspar. While many studies have demonstrated the ability of the method, analytical protocols vary significantly and to date no studies have provided an in-depth comparison and synthesis in terms of precision and accuracy. Here we compare four calibration protocols based on commonly used reference materials for Rb–Sr dating. We demonstrate that downhole fractionation trends (DHF) for natural biotite, K-feldspar and phlogopite contrast with that for the commonly used Mica-Mg nano-powder reference material. Consequently, Rb–Sr dates calibrated to Mica-Mg can be up to 5% inaccurate and the degree of inaccuracy appears to be unsystematic between analytical sessions. Calibrating to Mica-Mg also introduces excess uncertainty that can be avoided with a more consistent primary calibration material. We propose a calibration approach involving (1) NIST-610 glass as the

primary reference material (PRM) for normalization and drift correction and (2) a natural mineral with similar DHF characteristics to the analysed samples as matrix correction RM (MCRM) to correct the Rb/Sr ratio for matrix-induced offsets. In this work, MDC phlogopite (the source mineral for Mica-Mg nano-powder) was used as the MCRM, consistently producing accurate Rb–Sr dates for a series of natural biotites and K-feldspars with well-characterized expected ages. However, biotite from the Banalasta Adamellite, Taratap Granodiorite and Entire Creek pegmatite are also suitable RMs for Rb/Sr ratio calibration purposes with consistently <1.5% fully propagated uncertainties in our methodological approach. Until calibration using isochronous natural standards as the primary RM becomes possible in data-reduction software, the two-step calibration approach described here is recommended.

Keywords: reaction-cell ICP-MS; in-situ geochronology; Rb–Sr reference materials; calibration standards

1. Introduction

Rubidium-Strontium (Rb–Sr) geochronology using laser ablation – inductively coupled plasma – tandem mass spectrometry (LA-ICP-MS/MS) has become a popular method to constrain the formation or cooling age of potassium-bearing minerals (Gorojovsky and Alard, 2020; Hogmalm et al., 2017; Jegal et al., 2022; Kirkland et al., 2023; Larson et al., 2023; Laureijs et al., 2021; Li et al., 2020; Liebmann et al., 2022; Olierook et al., 2020; Redaa et al., 2021; Rosel and Zack, 2022; Sengun et al., 2019; Tillberg et al., 2021; Tillberg et al., 2020; Wang et al., 2022; Zack and Hogmalm, 2016). In contrast to traditional Rb–Sr dating involving column-chemistry in

specialized laboratories, the laser-ablation method allows rapid acquisition of Rb–Sr dates directly from thin sections or rock blocks with minimal sample preparation. The method involves the use of an ICP-MS/MS, equipped with a reaction cell where isobaric isotopes can be chemically separated due to their significant differences in reactivity with an introduced reaction gas (Balcaen et al., 2015 and references therein). Applied to Rb–Sr geochronology, CH_3F, SF_6, O_2 and N_2O have been used as reaction gasses (e.g. Hogmalm et al., 2017; Moens et al., 2001; Zack and Hogmalm, 2016), with the latter being the most widely used for quadrupole ICP-MS/MS due to its high reactivity. However, published analytical methodologies for LA-ICP-MS/MS Rb–Sr dating vary significantly beyond the applied reaction gas (Table 1). Reported laser conditions (fluence and repetition rate) are largely laser-wavelength dependent with common conditions being either ~5 - 7 J.cm^{-2} / 10 Hz for 213nm lasers, especially during initial development work (e.g. Hogmalm et al., 2017; Laureijs et al., 2021; Rosel and Zack, 2022; Sengun et al., 2019; Tillberg et al., 2020; Zack and Hogmalm, 2016) or ~2 - 4 J.cm^{-2} / 5 Hz for 193nm lasers (e.g. Kirkland et al., 2023; Larson et al., 2023; Li et al., 2020; Liebmann et al., 2022; Olierook et al., 2020; Redaa et al., 2021). The applied calibration protocols for mass discrimination and elemental fractionation, however, vary more significantly.

We define three types of reference materials (RM) in this manuscript:

(1) The Primary RM (PRM) has a homogenous isotopic composition and is used for normalisation and drift correction;

(2) The matrix correction RM (MCRM) has a heterogenous isotopic composition but well-known age and is used to correct the Rb/Sr ratio for systematic matrix-induced off-sets between the PRM and mineral samples.

(3) The secondary RM (SRM) has a well-known age and a similar composition to the analysed samples and is used to verify the accuracy of the calibration protocol.

Most published work uses a glass reference material as PRM, with NIST-610 being most popular to correct for drift and calibrate the Sr isotopic ratios. Rb/Sr ratios are most commonly calibrated against Mica-Mg, a phlogopite prepared as a pressed nano-powder pellet, regardless of the analysed mineral (micas in most published work). However, the approach varies, with some methods directly calibrating to Mica-Mg as the PRM (e.g. Gorojovsky and Alard, 2020; Hogmalm et al., 2017; Li et al., 2020; Redaa et al., 2021; Rosel and Zack, 2022; Sengun et al., 2019; Wang et al., 2022) and others using NIST-610 as the PRM followed by a correction for matrix-dependent fractionation against Mica-Mg as MCRM (e.g. Liebmann et al., 2022; Olierook et al., 2020). Secondary RMs, used to verify the accuracy of obtained dates, are either glass reference materials (e.g. Larson et al., 2023; Laureijs et al., 2021; Rosel and Zack, 2022) or in-house natural materials such as the La Posta biotite (Zack and Hogmalm, 2016), the MDC phlogopite (Redaa et al., 2021), or the CK001 biotite (Olierook et al., 2020).

In addition, laser-induced down-hole fractionation (DHF) can occur during ablation and aerosol condensation processes and is most apparent when ratioing elements with contrasting volatilities (e.g. Jackson and Günther, 2003; Košler et al., 2005; Longerich et al., 1996). Elemental Sr is more refractory than the volatile Rb and hence has a high potential to fractionate during laser ablation (Zack and Hogmalm, 2016). A small number of studies have directly compared different calibration approaches and have described differences in Rb–Sr DHF behaviour between commonly used reference materials (e.g. Redaa et al., 2021; Wang et al., 2022). However, systematic comparisons between data reduction protocols, tested with natural materials, are limited in the current literature. Here, we compare four different calibration approaches for a series of

natural biotite and K-feldspar samples. The samples were taken from quickly cooled igneous rocks, eliminating potential diffusion-related issues when comparing dates of different minerals. Hence, the well-constrained igneous crystallization ages are the expected reference ages for the analysed samples and one of the biotite samples has previously been dated by the Rb–Sr ID-TIMS method. The calibration approaches we compare are:

(A) NIST-610 as the PRM for both $^{87}Rb/^{87}Sr$ and $^{87}Sr/^{86}Sr$ ratios plus MDC phlogopite as MCRM;

(B) NIST-610 as the PRM for both $^{87}Rb/^{87}Sr$ and $^{87}Sr/^{86}Sr$ ratios plus Mica-Mg pressed pellet as MCRM;

(C) Mica-Mg as the PRM for $^{87}Rb/^{87}Sr$ ratios and NIST-610 as the PRM for $^{87}Sr/^{86}Sr$ ratios;

(D) Mica-Mg as the PRM for both $^{87}Rb/^{87}Sr$ and $^{87}Sr/^{86}Sr$ ratios

We discuss the differences between these approaches in terms of accuracy and precision, and highlight the importance of monitoring and correcting down-hole fractionation with appropriate reference materials.

2. Sample descriptions

2.1. MDC phlogopite and Mica-Mg nano powder

Mica-Mg nano-powder is used as a reference material for Rb–Sr dating. It consists of crushed phlogopite from Bekily (Madagascar) with a high Rb (1300 ± 40 $\mu g.g^{-1}$) and low Sr (27 ± 3 $\mu g.g^{-1}$) concentration (Redaa et al., 2023 and references therein). MDC is natural phlogopite, which was sourced from the same locality as Mica-Mg (Redaa et al., 2021). The reference age for both materials is 519.4 ± 6.5 Ma and the initial $^{87}Sr/^{86}Sr$ ratio is 0.72607 ± 0.0007 (2SE uncertainties),

constrained from a diopside (low-Rb mineral) that occurs in the same location (Hogmalm et al., 2017). However, for Mica-Mg some pellet to pellet variation in both Rb/Sr and Sr/Sr ratios has been observed (Jegal et al., 2022; Redaa et al., 2023).

2.2. Entire Creek pegmatite

The Entire Creek sample was taken from a deformed pegmatite in the Harts Range meta-igneous complex of central Australia, in the same location as described by Mortimer et al. (1987). The pegmatite cross-cuts folded and foliated amphibolites, is composed of coarse-grained quartz, plagioclase, alkali feldspar and biotite, with the latter defining a strong axial-plane foliation to folds outlined by the pegmatite. Biotite and whole-rock Rb/Sr and Sr/Sr isotope ratios, obtained by ID-TIMS at the University of Adelaide, are reported in Mortimer et al. (1987) and define a 7-point (3 biotite and 4 whole rock analyses) isochron age of 312.1 ± 1.8 / 5.1 Ma (95% confidence uncertainties, without / with overdispersion), recalculated in IsoplotR (Vermeesch, 2018), using the Villa et al. (2015) Rb–Sr decay constant of $1.3972 \pm 0.0045 \times 10^{-11}$ a^{-1} (Appendix 1).

2.3. Banalasta Adamellite (Bundarra Suite)

The S-type Banalasta Adamellite forms the southern end the Bundarra Batholith in the Southern New England Orogen in eastern Australia (e.g. Flood and Shaw, 1975; Jeon et al., 2012; Rosenbaum et al., 2012; Shaw and Flood, 1981). The Bundarra Batholith is an elongate north-south trending magmatic suite, spanning approximately 200 km. The Banalasta Adamellite is approximately 40 km in diameter and has sharp contacts with surrounding metasediments with a contact metamorphic aureole characterised by fine-grained cordierite-bearing assemblage at the pluton margin grading out to regional prehnite-pumpellyite metagreywacke assemblages over a distance of approximately 3 km (Flood and Shaw, 1977). Internally the granite is massive, coarse-

grained granitoid containing approximately equal proportions of K-feldspar and plagioclase, together with accessory apatite, zircon and monazite. Biotite predominantly occurs in multi-grain clots together with quartz, plagioclase, magnetite, zircon and apatite. In rare cases they contain relic garnet, suggesting they formed from hydration of garnet entrained from the granitic source region.

Melt-precipitated zircon from the Banalasta Adamellite gives zircon U-Pb ages of 286.2 ± 2.2 Ma (Black, 2007), 289.2 ± 1.7 Ma (Jeon et al., 2012) and 282 ± 4 Ma (Phillips et al., 2011). Whole rock Rb–Sr data from the Bundarra Suite give an age of 285 ± 15 Ma (n = 6/7, MSWD = 0.4). When additional feldspar Rb–Sr data are included in the isochron, the isochron age is 283 ± 10 Ma (n = 9/10, MSWD = 0.24) (Appendix 2). Both isochron dates were recalculated using the data from Flood and Shaw (1977) and the decay constant from Villa et al. (2015). Additionally, Hensel et al (1995) reported a model whole rock Rb–Sr age of 287 ± 10 Ma for a group of 16 samples from the Bundarra Suite. Overall, it is evident that Rb–Sr age data are similar to the ages of melt precipitated zircon, consistent with the lack of evidence for extended fractional crystallisation (Jeon et al 2012). The samples used in this study come from the same location as Black (2007) that has a granitic zircon of 286.2 ± 2.2 Ma, as well as a second location approximately 800 meters away.

2.4. Taratap Granodiorite

The Taratap Granodiorite in the Delamerian Orogenic belt in southern Australia is classified as S-type, calc-alkaline with a composition dominated by microcline megacrysts (c. 3–4 cm in length), which define a NNE-trending magmatic fabric in a coarse-grained groundmass of plagioclase,

154 quartz, K-feldspar and biotite, with accessory zircon, apatite, and monazite. Low-temperature
155 alteration is evident in thin section by the presence of chlorite–muscovite–titanite and minor
156 allanite (Burtt and Abbot, 1998). The sample was chosen for analysis because the timing of
157 emplacement is tightly constrained by a zircon U-Pb ID-TIMS age of 497.11 ± 0.56 Ma ($^{206}Pb/^{238}U$
158 weighted mean age, 95% confidence interval uncertainty, MSWD = 1.8, n = 6) and an apatite Lu-
159 Hf age of 497.1 ± 5.5 Ma (MSWD = 1.1, n = 38) (Glorie et al., 2023 and references therein).

160

161 **3. Analytical methods**

162 All Rb–Sr analyses were conducted at Adelaide Microscopy, University of Adelaide, using an
163 Agilent 8900x ICP-MS/MS, coupled to a RESOlution-LR ArF excimer (193 nm) laser ablation
164 system. A squid mixing device (Laurin Technic) was used to smooth the pulsed laser signal
165 between the laser and the mass-spectrometer. The instrument parameters follow those reported in
166 Redaa et al. (2021), with ablation in a He atmosphere (350 mL.min^{-1}), mixed with Ar (890 mL.min^{-1})
167 as the carrier gas and N_2 (3.5 mL.min^{-1}) added before the ICP torch to enhance the signal
168 sensitivity. N_2O (0.37 mL.min^{-1}) was used as the reaction gas to separate ^{87}Sr from ^{87}Rb. The ^{86}Sr
169 and ^{87}Sr isotopes were measured as their oxide reaction products (e.g. $^{87}Sr^{16}O$) with a mass shift
170 of 16 amu between the two quadrupole mass analysers (e.g. Q1 = 87 m/z, Q2 = 103 m/z). Despite
171 the high reaction efficiency of ^{87}Sr, residual unreacted Sr prevents direct measurement of ^{87}Rb.
172 Instead, ^{85}Rb was measured as a proxy for ^{87}Rb and calculated assuming natural isotopic
173 abundance. The samples and reference materials were ablated using a circular laser beam of 67
174 µm diameter, a fluence of 3.5 J.cm^{-2}, and repetition rate of 5 Hz. Further details are presented in
175 Table 2. A total of three analytical sessions were conducted, with largely identical instrumental
176 parameters between the different sessions. The ICP-MS was tuned to a sensitivity which kept Rb

177 in pulse mode in Mica-Mg (the material with the highest Rb concentration), negating the
178 requirement for additional pulse-analogue (P/A) corrections.
179 For each analytical session, NIST-610, Mica-Mg and MDC were used as reference materials for
180 calibration purposes. All data were processed in LADR (Norris and Danyushevsky, 2018) using
181 an in-built data reduction algorithm that calculates error correlations (Pearson correlation
182 coefficient) from the raw isotopic ratios for each sweep in an analysis, in the same way as for U-
183 Pb data reduction. Isotope ratios were calculated by: (1) background subtraction, (2) correcting
184 down-hole fractionation (DHF) against the PRM, (3) averaging the DHF corrected ratios of each
185 sweep in the analysis, and then (4) normalising to the PRM to correct for matrix independent
186 instrument mass bias and drift. LADR applies a robust uncertainty propagation using the total
187 uncertainty budget of the measured quantified ratios. An example of an `uncertainty tree`, which
188 can be queried for every analysis, is given in Appendix 3. The reader is referred to the LADR
189 software manual (https://norsci.com/?p=ladr-support) for further details.
190 Normalisation of the measured Rb/Sr and Sr/Sr ratios was conducted with two different reference
191 materials (NIST-610 and Mica-Mg), following the four analytical protocols outlined above (A-D).
192 The reference $^{87}Rb/^{87}Sr$ and $^{86}Sr/^{87}Sr$ ratios used for Mica-Mg were 83.4 ± 1.0 and 0.53981 ±
193 0.00070, respectively (Hogmalm et al., 2017). For NIST-610, the $^{87}Rb/^{87}Sr$ was calculated from
194 concentration data (GeoREM preferred values) as 3.28 ± 0.03 and for the $^{86}Sr/^{87}Sr$ ratio, the
195 reference value of 1.409048 ± 0.000036 was used (Woodhead and Hergt, 2001). For each
196 normalization protocol, DHF corrections of the $^{87}Rb/^{87}Sr$ ratios were applied based on the DHF
197 behaviour of the applied PRM. No DHF correction was applied to the $^{86}Sr/^{87}Sr$ ratios. Where
198 NIST-610 was used as the PRM, MDC phlogopite or Mica-Mg were used as MCRM to correct

199 the $^{87}Rb/^{87}Sr$ ratios for matrix-dependant fractionation (cfr. Roberts et al., 2017 for U/Pb ratios;
200 Simpson et al., 2022 for Lu/Hf ratios).
201 All mica samples (including biotite samples and MDC phlogopite) were ablated with the laser
202 ablating parallel to cleavage. The Bundarra and Taratap samples were analysed in thin section and
203 optical microscopy (birefringence) was used to only select ablation targets with upright (± 10°)
204 cleavage. The coarse Entire Creek biotites were mounted as mica-books using a vice to prevent
205 air-gaps between individual mica sheets, with the mica sheets mounted upright exposing multiple
206 cleavage planes perpendicular to the surface.
207 For each sample and reference material, inverse isochron Rb–Sr dates (Li and Vermeesch, 2021)
208 were calculated in IsoplotR (Vermeesch, 2018), based on the processed $^{87}Rb/^{87}Sr$ and $^{86}Sr/^{87}Sr$
209 ratios, their 2SE uncertainties, and the calculated error correlations. Reported inverse isochron
210 uncertainties are fully propagated 95% confidence intervals, including the uncertainty on the decay
211 constant and added uncertainty for overdispersion where required (calculated in IsoplotR). The
212 exceptions are the inverse isochron dates for MDC and Mica-Mg when used as MCRMs, which
213 are used to correct the Rb/Sr ratios after calibrating to NIST-610. For these cases the reported
214 uncertainties are 95% confidence uncertainties without external uncertainties (as the external
215 uncertainties would otherwise be applied twice to the isochron dates of the analysed samples).
216 Session-dependant correction factors (CF) were calculated from the measured $^{87}Rb/^{87}Sr$ ratio for
217 MDC and Mica-Mg (after drift corrections) and compared to the reference value (calculated from
218 the published age for both MDC and Mica-Mg of 519.4 ± 6.5 Ma; Hogmalm et al., 2017; Redaa
219 et al., 2021). These CF values (= measured ratio/expected ratio) were subsequently applied to each
220 unknown analysis when calibrated to either MDC or Mica-Mg. Finally, the uncertainties on the

MDC and Mica-Mg dates are propagated to the reported Rb–Sr isochron uncertainties for each NIST-610 calibrated sample using the quadratic addition of the relative uncertainties.

4. Results

4.1. Downhole fractionation trends

In this section, we compare the downhole fractionation (DHF) trend of the $^{87}Rb/^{87}Sr$ ratio between the analysed feldspars and micas and the reference materials (NIST-610 and Mica-Mg) (Fig. 1). The obtained fractionation trends do not vary significantly between different sessions; however, data from analytical session 3 are presented as this session contains data for all analysed samples presented in this paper. The DHF trends were calculated in LADR and individual scatter plots can be found in Appendix 4. As shown, The DHF trends for the analysed biotite, phlogopite and K-feldspar samples are internally consistent, showing ~10% increase in Rb/Sr ratio over the first 20 s of ablation, followed by a flatter trend in the subsequent 20 s. NIST-610 shows a similar trend of increasing Rb/Sr ratio with ablation time, however the amplitude of the DHF curve is more subdued compared to the natural samples (~3.5% increase in the first 20 s ablation). In contrast, the DHF pattern for Mica-Mg shows an oscillating trend, increasing for the first ~10 s of ablation and then dropping for the subsequent ~30 s of ablation (Fig. 1).

4.2. Within-session reproducibility of $^{87}Rb/^{87}Sr$ and $^{86}Sr/^{87}Sr$ ratios

Figure 2 shows the within-session variability (prior to drift correction) of the $^{87}Rb/^{87}Sr$ and $^{86}Sr/^{87}Sr$ ratios for both PRMs NIST-610 and Mica-Mg in analytical session 3. The reference materials are considered homogenous in both isotopic ratios, meaning that any variations are

purely due to differences in the ablation characteristics from spot to spot. As shown, the measured $^{87}Rb/^{87}Sr$ ratios and $^{86}Sr/^{87}Sr$ ratios are significantly more consistent for NIST-610 compared to Mica-Mg (both measured using the same analytical conditions and spot size). The maximum within-session variability (=min-max range) in the $^{87}Rb/^{87}Sr$ ratio is < 3% for NIST-610, compared to > 8% for Mica-Mg. The $^{86}Sr/^{87}Sr$ ratio is more consistent for both RMs, however, the uncertainty on individual analyses is approximately 3× larger for Mica-Mg compared to NIST-610. ICP-MS mass-bias drift is minimal for both isotope ratios in NIST-610, with only a slight increase in the Rb/Sr ratio over the first 2-3 hours of analysis. As both Mica-Mg and NIST-610 were analysed sequentially in the same analytical session, the apparent 'drift' in the Mica-Mg $^{86}Sr/^{87}Sr$ ratios are due to variations in ablation rather than changes in the ICP-MS mass bias.

4.3. Isochron Rb–Sr dates for natural K-feldspars and micas

Inverse isochron plots and resulting Rb–Sr dates are presented for each analytical protocol in Appendix 5. Summary plots are shown in Figure 3. The data table with the input $^{87}Rb/^{87}Sr$ and $^{86}Sr/^{87}Sr$ ratios is accessible from Figshare via the link in the data availability section. For the Bundarra samples, the biotite isochrons are anchored to apatite Rb/Sr ratios, given that the apatites commonly occur as inclusions within biotite. For the K-feldspars, the isochrons are anchored to plagioclase, given that the analysed K-feldspars often show minor exsolution with plagioclase. However, the choice of anchoring mineral gives no difference in the obtained biotite and K-feldspar inverse isochron Rb/Sr dates. For the Taratap sample, isochron anchoring was conducted to a combination of plagioclase and apatite in session 1, but only plagioclase in sessions 2 and 3, given the limited occurrence of apatite in thin section. For the Entire Creek biotite sample, anchoring was conducted to whole-rock $^{86}Sr/^{87}Sr$ ratios from Mortimer et al. (1987). The MDC

and Mica-Mg isochrons were anchored to an initial $^{86}Sr/^{87}Sr$ ratio of 1.3773 ± 0.0013 and calibrated to the published age of 519.4 ± 6.5 Ma (Hogmalm et al., 2017; Redaa et al., 2021).

The summary of obtained inverse Rb–Sr dates is presented in Table 3. As shown, there is only marginal variation in the absolute biotite dates between the three analytical protocols involving Mica-Mg, either as the PRM for Rb/Sr ratios (protocols C & D) or as a MCRM (protocol B). Hence, in order to evaluate the accuracy of the obtained Rb–Sr dates against the expected references ages for each sample, we only compare the first two analytical protocols (NIST-610 as the PRM and either: (A) MDC or (B) Mica-Mg as MCRM).

Figure 4 compares the obtained Rb–Sr inverse isochron dates to the expected ages for the three samples, that were analysed over two or three analytical sessions. The uncertainties for the K-feldspar dates are not shown as they are too large to be useful (due to the relatively low radiogenic nature of typical K-feldspar versus micas), here we only compare the accuracy of the absolute dates. As shown, analytical protocol (A) involving NIST-610 as PRM and MDC phlogopite as MCRM consistently gives the most accurate Rb–Sr dates across all different analytical sessions. For this analytical protocol, the Rb–Sr biotite dates for the Bundarra samples are 287.1 ± 2.4 Ma, 284.7 ± 3.0 Ma, 287.7 ± 2.3 Ma and 285.7 ± 2.6 Ma (between two samples over two analytical sessions), which are in excellent agreement with the published zircon U-Pb age of 286.2 ± 2.2 Ma (Black, 2007) from the same outcrop. The K-felspar dates of 290 ± 14 Ma, 285 ± 15 Ma, 290 ± 37 Ma and 288 ± 37 Ma are in excellent agreement as well but are less useful to evaluate age accuracies given their larger uncertainties. Similarly for the Taratap sample, the obtained biotite Rb–Sr dates of 499.4 ± 3.6 Ma and 495.7 ± 4.0 Ma as well as the (imprecise) K-feldspar Rb–Sr dates of 500 ± 30 Ma, 501 ± 50 Ma and 495 ± 35 Ma are in excellent agreement with the zircon U-Pb ID-TIMS age of 497.1 ± 0.6 Ma as well as the apatite Lu-Hf age of 497.1 ± 5.5 Ma for the

same sample (Glorie et al., 2023). Hence, the combined dataset suggests that the biotite, K-feldspar and zircons record the same (crystallization) age for both the Bundarra and Taratap samples. The Entire Creek biotite gave consistent Rb–Sr dates of 310.7 ± 1.5 Ma and 311.6 ± 3.1 Ma, in excellent agreement with the ID-TIMS age of 312.1 ± 1.8 / 5.1 Ma (95% confidence uncertainties, without / with overdispersion), based on the Rb/Sr ratios in Mortimer et al. (1987), recalculated with the Villa et al. (2015) Rb–Sr decay constant.

5. Discussion

5.1. Downhole fractionation corrections

Few previous studies have reported Rb–Sr DHF trends for a series of artificial reference materials (i.e. glass standards and pressed pellets; Redaa et al., 2021; Wang et al., 2022). However, to the best of our knowledge, DHF trends have not been evaluated for natural materials with the exception of phlogopite MDC (Redaa et al., 2021). In our experiments, DHF is more pronounced in natural micas and K-feldspar than observed for the NIST-610 glass and Mica-Mg pressed pellet, when ablated under the same analytical conditions (Fig. 1). Comparatively, Mica-Mg appears least appropriate to correct the analysed samples for DHF, given its systematically different DHF trend. NIST-610 shows less DHF compared to the analysed micas and K-feldspars but its trend is more systematic (similar shape with lower amplitudes). Thus, correcting for DHF against NIST-610 reduces the observed DHF for the analysed samples, while Mica-Mg significantly under-corrects for DHF or accentuates it when applied to minerals. MDC biotite would be the most appropriate choice for DHF correction as it behaves very similar to the analysed mica and K-feldspar samples. However, as with most natural materials, MDC is not sufficiently homogenous in $^{87}Rb/^{87}Sr$ ratio to be used as a PRM. While the shape or slope of DHF trends can vary depending on laser conditions (spot size, frequency and fluence), it cannot be eliminated for elements with contrasting

311 volatilities such as Rb and Sr. However, based on the presented data, the use of NIST-610 is the
312 more appropriate reference material to correct for DHF and Mica-Mg would exacerbate instead of
313 reduce the effects of DHF.
314 If no DHF correction is applied, accurate data can only be achieved if exactly the same signal
315 interval is selected in both the RM and sample. If there is a residual DHF slope on the sample
316 Rb/Sr ratios that is different to the RM (e.g. crystalline material versus Mica-Mg), then selecting
317 a shorter signal interval can significantly bias Rb/Sr ratios and hence the apparent age.
318

319 **5.2. Mica-Mg vs NIST-610 and MDC as calibration standards**

320 **5.2.1. Uncertainty comparisons**

321 The contributions to the propagated uncertainties of individual analyses from the reference
322 materials (average signal precision and calibration curve misfit) are much larger when calibrating
323 to Mica-Mg compared to NIST-610 for both $^{87}Rb/^{87}Sr$ and $^{86}Sr/^{87}Sr$ ratios (Fig. 5). For example,
324 in analytical session 1, the obtained uncertainties for individual $^{87}Rb/^{87}Sr$ ratios for the Entire
325 Creek biotite sample are more than double when using Mica-Mg compared to NIST-610 as the
326 PRM (Fig. 5). As a result, the choice of Mica-Mg instead of NIST-610 as the PRM will increase
327 the uncertainties on each analysis, and might consequently mask the presence of multiple data
328 populations. It will also introduces excessive uncertainties onto the calculated isochron dates.

329 The use of Mica-Mg as calibration standard for $^{86}Sr/^{87}Sr$ ratios most significantly affects the
330 isochron precision of low-radiogenic samples such as K-feldspar samples. As shown in Table 3
331 and Figure 5, the uncertainty on the K-feldspar isochron dates can be up to 2× larger, compared to
332 other calibration methods. Furthermore, the resulting MSWD values on the isochron regressions
333 are consistently < 0.3 (Table 3), suggesting excessive uncertainties on individual data points. For

334 the more radiogenic biotite samples, the larger uncertainties in $^{86}Sr/^{87}Sr$ ratios have negligible
335 effects to the precision on the isochron dates.

336 The precision of the calibrated $^{87}Rb/^{87}Sr$ ratios is more important to the isochron uncertainty of
337 highly radiogenic materials, such as most types of micas. Calibrating to NIST-610 versus Mica-
338 Mg yields either more precise biotite isochron dates or identical precision. However, when NIST-
339 610 is used as the PRM, uncertainty propagation from the MCRM (MDC or Mica-Mg) leads to
340 either identical or slightly worse isochron uncertainties compared to using Mica-Mg as PRM (Fig.
341 5; Table 3). The difference relates to the degree of overdispersion. The larger uncertainties on the
342 Rb/Sr ratios when using Mica-Mg as PRM result in lower MSWD values, reducing the uncertainty
343 on the isochron regression. This excess uncertainty when calibrating to Mica-Mg might mask
344 meaningful geological scatter in Rb/Sr ratios and it is, therefore, advisable to produce isochrons
345 based on data with the best possible analytical precision.

346 In summary, Mica-Mg should not be used as calibration standard for $^{86}Sr/^{87}Sr$ ratio calculations
347 for low-radiogenic samples as it introduces excessive uncertainties to age calculations. For high-
348 radiogenic samples, using Mica-Mg as the PRM also introduces larger uncertainties to individual
349 data points compared to using NIST-610, but there is no significant difference in propagated
350 uncertainty after secondary correction to either MDC or Mica-Mg. For Rb/Sr ratio calibrations,
351 NIST-610 is more consistent, resulting in lower uncertainties on individual Rb/Sr ratios. When
352 there is no overdispersion, this results in better isochron age precision. However, overdispersion
353 can be masked by the increased uncertainties on Rb/Sr ratios, resulting in better apparent precision
354 when data are calibrated to Mica-Mg.

355 **5.2.2. Accuracy comparisons**

356 It has been observed previously that Rb–Sr dates are offset from their expected ages when
357 calibrated to the NIST-610 reference material (e.g. Gorojovsky and Alard, 2020; Wang et al.,
358 2022). In contrast, Mica-Mg seems to better reproduce expected ages, although the significant
359 uncertainties obtained for natural materials in previous studies render appropriate accuracy testing
360 difficult. For example, Wang et al. (2022) compares measured to expected Rb–Sr dates for three
361 samples with known ages. The best achieved uncertainty in their experiment was ~2.6% for one
362 sample, while for the other samples the reported uncertainties are ~5.6 and 6.3 %. Similarly, the
363 accuracy comparisons in Gorojovsky and Alard (2020) use the Monastery phlogopite, with a
364 precision of ~4% when calibrated to Mica-Mg. Both papers report data normalized to NIST-610
365 but do not apply a secondary correction for matrix-dependent fractionation.
366 For the biotites analysed in our study, the fully propagated 95% confidence interval uncertainties
367 ranges between 0.8 and 1.6% when calibrated to Mica-Mg and between 1.0% and 1.4% when
368 calibrated to NIST-610 and corrected to MDC (depending on the sample and analytical session;
369 Table 3), allowing for more detailed accuracy comparisons. Figure 4 illustrates that using NIST-
370 610 and MDC as calibration reference materials produces the most accurate results, compared to
371 the expected references dates. For the biotite results, the obtained Rb–Sr dates are within 0.5%
372 accuracy compared to the expected ages. The K-feldspar dates are accurate within 1%, except for
373 session 2, where accuracy is within 1.5%. When the same data are calibrated against Mica-Mg
374 (either using NIST-610 as the PRM and Mica-Mg as MCRM, or directly using Mica-Mg as the
375 PRM), the results are significantly offset from their expected ages. For the biotite results calibrated
376 to Mica-Mg, accuracy is within 2% for sessions 2 and 3 and there is 5% age off-set in session 1.
377 For the K-felspars, the age offset is up to 2.5% in sessions 2 and 3 and 6% in session 1. While the

age offsets in sessions 2 and 3 might be regarded as `acceptable`, given the obtained precision, the more significant inaccuracy in session 1 renders Mica-Mg to be less desirable as a PRM.

The difference in accuracy between session 1 and sessions 2 and 3 can be explained by the difference in measured dates for the MDC and Mica-Mg reference materials, normalised to NIST-610. For sessions 2 and 3, MDC and Mica-Mg produced similar isochron dates (2.3 and 1.9% difference respectively) (Table 3; Fig. 6). For session 1, however, MDC gives a significantly different age (494 ± 4 Ma) compared to Mica-Mg (469 ± 4 Ma). These differences in accuracy (ca. 5 % in session 1 and ca. 2 % in sessions 2 and 3) are in line with the observed age off-sets between the measured dates and reference dates for the biotite and K-feldspar samples, calibrated to Mica-Mg.

5.2.3. Long-term comparison between MDC and Mica-Mg as secondary calibration standards

Given that the accuracy of the Rb–Sr method appears to be significantly dependent on the applied calibration reference materials, and that the measured Rb–Sr dates of these calibration standards fluctuate significantly between analytical sessions when compared to NIST-610, the long-term behaviour of the MDC and Mica-Mg reference materials needs to be evaluated. Figure 7 presents 2.5 years of measured Rb–Sr dates for MDC and Mica-Mg, both calibrated to NIST-610 as the PRM. All data in this plot have been processed identically. The Rb–Sr dates for Mica-Mg are generally more consistent, ranging between ca. 462 and 479 Ma, with a standard deviation of 4.5 Ma, while the MDC dates show more variation, ranging between ca. 465 and 494 Ma, with a standard deviation of 7.7 Ma. In all but two sessions, MDC produces an older Rb–Sr date compared to Mica-Mg. The analytical sessions discussed above are highlighted in Figure F and encompass

401 the maximum variability in measured Rb–Sr dates for MDC. With the premise that calibration to
402 NIST-610 and MDC produces accurate Rb–Sr dates (as discussed in section 5.2.2), the difference
403 between the measured MDC and Mica-Mg dates (Fig. 6, 7) can be regarded as an estimate of the
404 degree of inaccuracy when data are calibrated to Mica-Mg. While some sessions reveal very little
405 off-set between both standards, using Mica-Mg as calibration standard can lead to up to 5%
406 inaccuracy in Rb–Sr dates. The cause of the observed variability is currently unknown, however,
407 in the second-to-last session with a significantly older Mica-Mg date compared to MDC, the
408 analysed samples might have received a lower effective laser fluence compared to other sessions
409 as the glass between the laser beam and samples was not cleaned prior to analysis. The lower
410 fluence could change the effective matrix bias between NIST-610, Mica-Mg and MDC, however,
411 calibration of biotite against MDC produces accurate results as demonstrated in section 5.2.2. In
412 contrast, although Mica-Mg produces more consistent Rb–Sr dates between analytical sessions,
413 these dates are unreliable given the variable and unsystematic degree of inaccuracy between
414 sessions.
415

416 **6. Conclusions**

417 Based on our observations, the use of Mica-Mg as calibration reference material is not
418 recommended, for the following reasons:
419 (1) The down-hole fractionation (DHF) trend for Mica-Mg is not comparable with the DHF
420 trends of natural bitote, phlogopite and K-feldspar (Fig. 1). Using Mica-Mg to correct DHF
421 would exacerbate instead of reduce DHF in those minerals;

(2) Given the relatively poor reproducibility of $^{87}Rb/^{87}Sr$ ratios and significant uncertainty on individual $^{87}Sr/^{86}Sr$ measurements (Fig. 2), Mica-Mg as PRM or MCRM introduces excess uncertainty that can be avoided using a more consistent PRM such as NIST-610;

(3) We demonstrated that calibrating to Mica-Mg may lead to up to 5% inaccuracy in Rb–Sr age (Fig. 4, 6, 7) and that the degree of inaccuracy is unsystematically session-dependant.

We suggest a different approach, involving (1) calibration of the $^{87}Rb/^{87}Sr$ and $^{87}Sr/^{86}Sr$ ratios to a primary reference material with high Rb and Sr concentrations and homogenous isotopic ratios such as NIST-610 glass, including DHF correction of the Rb/Sr ratios, followed by (2) a correction of the $^{87}Rb/^{87}Sr$ ratio to a natural mineral MCRM with a similar DHF trend as the samples to be analysed. In our observations with a 67µm spot-size, there are no significant differences in matrix effects comparing biotite, phlogopite and K-feldspar, suggesting that any of these natural minerals as MCRM can produce accurate dates for K-rich minerals. We have used MDC phlogopite as MCRM and demonstrate accurate Rb–Sr dates for a range of biotites and K-feldspars with well-established age constraints. For the biotite dates, the fully propagated uncertainties are <1.5 %, allowing accuracy verifications at high analytical precision. The K-feldspar dates have relative high uncertainties (ca. 5-10%) and, therefore, the accuracy of the calibration cannot robustly be tested. However, absolute values agree with biotite dates and for a given sample, biotite and K-feldspar analyses statistically constitute a single isochron.

Finally, while this two-step calibration protocol is currently recommended due to current constraints with data processing software, new developments involving calibrating to isochronous reference materials might become the desired approach in the future.

Data availability

The Rb–Sr dataset used in this manuscript is freely available on figshare at https://doi.org/10.25909/23996484.

Acknowledgements

This paper was supported by research grants FT210100906 and DP220103037 from the Australian Research Council (ARC). Janne Liebmann and Nick Roberts are thanked for their constructive reviews.

Author contributions

SG: Conceptualization, investigation, writing – original draft, methodology, funding acquisition, visualisation, formal analysis

SEG: Conceptualization, investigation, writing – review and editing, methodology

MH: Conceptualization, investigation, writing - review and editing, resources

JCL: Conceptualization, investigation, writing - review and editing, formal analysis

Competing interests

The authors declare that they have no conflict of interest.

Ethical statement

This manuscript is an original work that is not submitted or published elsewhere.

468 **Tables**

	React. gas ($ml.min^{-1}$)	Laser wavel. (nm)	Fluence ($J.cm^{-2}$)	Rep. rate (Hz)	Spot (µm)	Rb-Sr calibration	Sr-Sr calibration	DHF	Err. corr.
Zack and Hogmalm 2016	O_2 (0.25)	213	7	10	80	Pl: NIST-610; Ksp: BCR-2G; Bt: La Posta	NIST-610	No	No
Hogmalm et al. 2017	O_2 (0.25) N_2O (0.16) SF_6 (0.04)	213	O_2: 7 N_2O: 6-8 SF_6: 6-8	10 4-5 10	80 50 50	Mica-Mg	NIST-610	No	No
Tillberg et al. 2020	N_2O (?)	213	?	?	50	BCR-2G (Sec: Mica-Mg/La Posta)	NIST-610	No	Yes
Rösel and Zack 2022	N_2O (0.18-0.20)	213	5-7	10	50-60	Mica-Mg (sec: NIST-610 / BCR-2G)	Mica-Mg	No	No
Gorojovsky and Alard 2020	N_2O (0.25)	193 and 213	7.8	5	85	Mica-Mg	Mica-Mg, NIST-610, BHVO-2G	No	No?
Larson et al 2023	N_2O (0.37)	193	4	10	50	Mica-Mg (Sec: Mica-Fe)	NIST-610	Yes?	Yes
Laureijs et al. 2021	CH_3F (10%)	213	6	10	50	ATHO-G, T1-G, StHs6/80-G	NIST-612	No	Yes
Li et al. 2020	N_2O (0.35)	193	3.5	5	74	Mica-Mg Sec: MDC	Mica-Mg	No	No
Liebmann et al. 2022	N_2O (?)	193	2.5	5	64	NIST-610 + Mica-Mg Sec: CK001 bt	NIST-610	No	Yes
Olierook et al. 2020	N_2O (0.25)	193	2.5	5	64-87	NIST-610 + Mica-Mg Sec: CK001 bt	NIST-610	No	No
Redaa et al. 2021	N_2O (0.37)	193	3.5	5	74	Mica-Mg Sec: MDC	Mica-Mg	monitored	No
Sengun et al. 2019	N_2O (?)	213	5.7	10	50	Mica-Mg	NIST-610	No	No
Tilberg et al. 2021	N_2O (?)	213	?	?	50	Mica-Mg / NIST 610	NIST-610	No	Yes
Wang et al. 2022	N_2O (0.25)	193	7	5	85	Mica-Mg	NIST-610, BHVO-2G, BCR-2G	monitored	No
Kirkland et al. 2023	N_2O (0.25)	193	2	5	64	Mica-Mg Sec: CK001 bt	NIST-610	No	No

Table 1: Summary of published analytical conditions and protocols for LA-ICP-MS/MS Rb–Sr dating. Rep. rate = laser repetition rate; Sec = secondary reference material; Bt = biotite; ksp = K-feldspar; Pl = plagioclase; Err. Corr. = error correlation calculated (in most cases based on calculated uncertainties after data-reduction rather than during data-reduction); In case of method development work - `best conditions` are quoted.

Laboratory	Adelaide Microscopy – The University of Adelaide
Laser ablation system	RESOlution-LR ArF excimer laser
ICP-MS instrument	Agilent 8900x ICP-MS/MS
Analytical method – materials	*in situ* Rb-Sr - biotite, K-feldspar, plagioclase (anchor), apatite (anchor)
Sample preparation	mineral separates in 1-inch resin mounts and thin sections
Plasma Settings	
RF power	1350 W
Sample Depth	5.0 mm
Ar carrier gas	0.89 L/min
He carrier gas	0.38 L/min
N_2 addition	4 mL/min
Lens Parameters	
Extract 1	1.5 V
Extract 2	-80 V
Omega Bias	-85 V
Omega Lens	5.0 V
Q1 entrance	-10 V
Q1 exit	-2.0 V
Cell focus	-2.0 V
Cell Entrance	-90 V
Cell Exit	-120 V
Deflect	10 V
Plate Bias	-80 V
Q1 bias	-2.0 V
Q1 Prefilter Bias	-10.0 V
Q1 Postfilter Bias	-10.0 V
N_2O gas flow	0.37 mL/min
Octopole bias	-6.0 V
Axial Acceleration	2.0 V
Octopole RF	180 V
Energy Discrimination	-7.0 V
Analysis Parameters	
Laser Wavelength	193 nm
Laser fluence	3.5 J/m2
Sample laser diameter	67 µm
Laser repetition rate	5 Hz
Background duration	30 s
Analysis duration	40 s
Isotopes measured & dwell times (ms)	^{23}Na (2), ^{24}Mg (2), ^{27}Al (2), $^{29+16}$Si (2), $^{31+16}$P (2), ^{39}K (2), $^{43+16}$Ca (2), ^{55}Mn (2), $^{56+16}$Fe (2), ^{85}Rb (10), $^{86+16}$Sr (50), $^{87+16}$Sr (50), $^{88+16}$Sr (50), $^{89+16}$Y (5), $^{90+32}$Zr (5), $^{93+32}$Nb (5), all $^{x+16}$REE (5), $^{232+15}$Th (5), $^{238+16}$U (5)

Table 2: Analytical conditions for the three LA-ICP-MS/MS sessions in this paper.

			(A) NIST-610 + MDC		(B) NIST610 + Mica-Mg		(C) Mica-Mg & NIST-610		(D) Mica-Mg	
Sample (exp. age)	S	n	Age (± 2σ) [Ma]	MS WD	Age (± 2σ) [Ma]	MS WD	Age (± 2σ) [Ma]	MS WD	Age (± 2σ) [Ma]	MS WD
Ent Crk Bt	1	24	310.7 ± 1.5/2.5/3.1	1.1	327.8 ± 1.7/2.7/3.2	0.96	327.6 ± 3.3/3.9	0.27	328.8 ± 3.4/4.0	0.25
(312.1 ± 1.8[1])	3	20	311.6 ± 3.1/3.8/4.5	2.5	317.6 ± 3.2/3.8/4.6	2.4	316.1 ± 3.2/3.8	0.85	316.2 ± 3.2/3.8	0.84
Bund1b Bt	2	44	287.1 ± 1.6/2.4/3.4	1.6	280.3 ± 1.5/2.4/3.2	1.7	280.1 ± 1.6/2.4	0.97	280.2 ± 1.6/2.4	0.82
(286.2 ± 2.2[2])	3	22	284.7 ± 2.4/3.0/3.8	1.0	290.1 ± 2.5/3.1/3.8	1.1	288.4 ± 4.1/4.5	0.7	288.2 ± 4.3/4.7	0.28
Bund1b Ksp	2	57	290 ± 14/14/14	0.87	284 ± 14/14/14	0.88	284 ± 14/14	0.84	280 ± 23/23	0.3
(286.2 ± 2.2[2])	3	53	287 ± 15/15/15	0.88	292 ± 15/15/15	0.88	290 ± 15/16	0.86	283.4 ± 38/38	0.19
Bund6a Bt	2	38	287.7 ± 1.3/2.3/3.4	1.4	280.9 ± 1.3/2.2/3.1	1.5	279.5 ± 1.5/2.3	0.71	279.5 ± 1.5/2.3	0.7
(286.2 ± 2.2[2])	3	22	285.7 ± 1.9/2.6/3.4	0.74	291.2 ± 1.9/2.7/3.6	0.72	288.7 ± 3.5/4.0	0.54	288.8 ± 3.6/4.0	0.34
Bund6a Ksp	2	45	290 ± 37/37/37	0.69	283 ± 36/36/36	0.69	281 ± 36/36	0.68	283 ± 75/75	0.16
(286.2 ± 2.2[2])	3	40	288 ± 37/37/37	0.65	293 ± 38/38/38	0.65	294 ± 39/39	0.65	296 ± 93/93	0.11
Taratap Bt	2	30	499.4 ± 1.8/3.6/5.6	1.2	487.7 ± 1.7/3.5/5.2	1.2	489.6 ± 2.8/4.2	0.67	489.6 ± 2.8/4.2	0.63
(497.1 ± 0.6[3])	3	16	495.7 ± 2.5/4.0/5.5	1.2	505.1 ± 2.6/4.1/5.8	1.2	504.0 ± 5.4/6.3	0.51	504.0 ± 5.5/6.3	0.52
Taratap Ksp	1	54	500 ± 30/30/30	0.53	527 ± 31/31/31	0.53	527 ± 32/32	0.50	539 ± 58/58	0.14
(497.1 ± 0.6[3])	2	20	501 ± 50/50/50	0.58	490 ± 49/49/49	0.58	492 ± 50/50	0.56	494 ± 106/106	0.12
	3	18	495 ± 35/35/35	0.95	504 ± 36/36/36	0.95	490 ± 39/39	1.1	511 ± 63	0.3

			NIST-610 as PRM	
MCRM	S	n	Age (± 2σ) [Ma]	MS WD
MDC	1	34	494.4 ± 3.0	1.4
	2	21	464.5 ± 4.0	1.3
	3	30	470.6 ± 3.6	1.1
Mica-Mg	1	35	468.6 ± 2.5	2.8
	2	21	475.7 ± 3.7	3.5
	3	20	461.8 ± 3.7	2.7

Table 3: Summary table of Rb–Sr dates obtained in this study. S = session number, n = number of analysed grains, exp. age = expected reference age (see below). All uncertainties are 95% confidence intervals and are reported as (1) excluding external uncertainty (on the decay constant) / (2) including external uncertainties / (3) with propagated uncertainty from the correction standard (for methods (A) and (B) only). (A) NIST-610 as PRM and MDC as MCRM to calibrate Rb/Sr ratios; (B) NIST-610 as PRM, Mica-Mg as MCRM to calibrate Rb/Sr ratios; (C) Rb/Sr ratios calibrated to Mica-Mg as PRM and Sr/Sr ratios calibrated to NIST-610 as PRM; (D) Mica-MG as PRM for both Rb/Sr and Sr/Sr ratios. [1] Rb-Sr TIMS age from Mortimer et al. (1987), recalculated with Villa et al. (2015) decay constant in IsoplotR (Vermeesch, 2018). The reported uncertainty is 95% confidence interval but does not take overdispersion into account. [2] Zircon U-Pb age for the Banalasta Adamellite in the Bundarra Suite, from Black (2007). [3] Zircon U-Pb TIMS age for the Taratap Granodiorite, reported in Glorie et al. (2023).

Figures

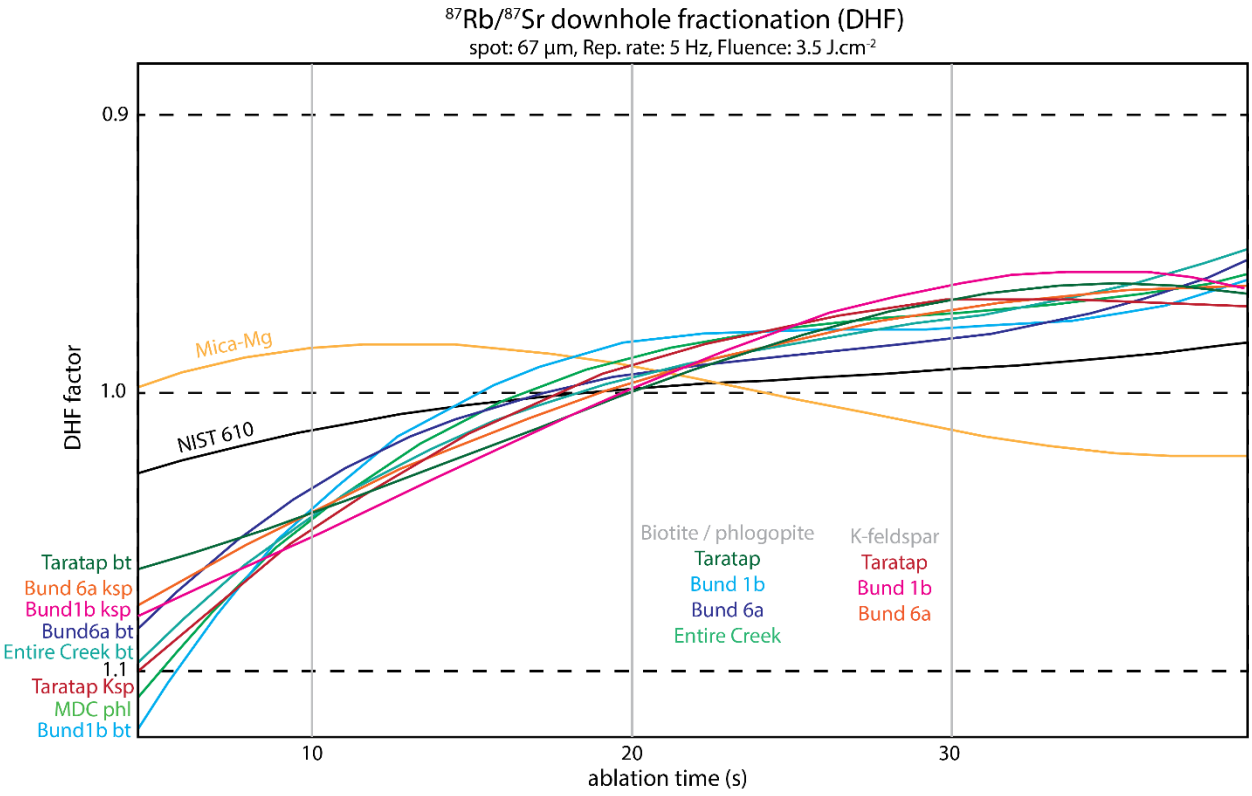

Figure 1: $^{87}Rb/^{87}Sr$ downhole fractionation profiles for the analysed reference materials Mica-Mg (yellow line) and NIST-610 (black line), the biotite / phlogopite (green-blue lines) and K-felspar (red-pink lines) samples in analytical session 3, calculated in LADR (Norris and Danyushevsky, 2018). The DHF factor is calculated relative to the average ratio of the ablation signal (i.e. DHF factor of 1 = average $^{87}Rb/^{87}Sr$ ratio of the downhole signal).

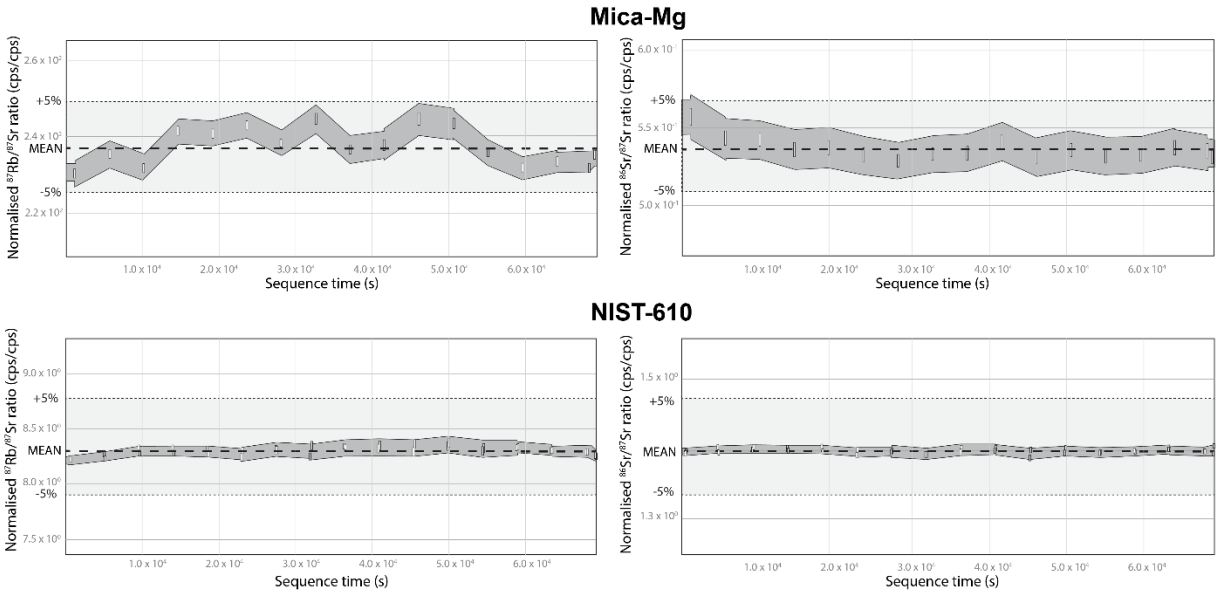

500

501 **Figure 2:** Variability of the $^{87}Rb/^{87}Sr$ and $^{86}Sr/^{87}Sr$ ratios for the analysed reference materials
502 NIST-610 and Mica-Mg over the total duration of analytical session 3 (prior to drift correction).
503 All plots are scaled equally to ± 5% variation of the mean to aid visual comparisons. The vertical
504 bars are ±1 standard deviation. The gray envelopes models ±2 standard deviation (note that for
505 NIST-610 each standard was measured twice at each standard bracket).

506

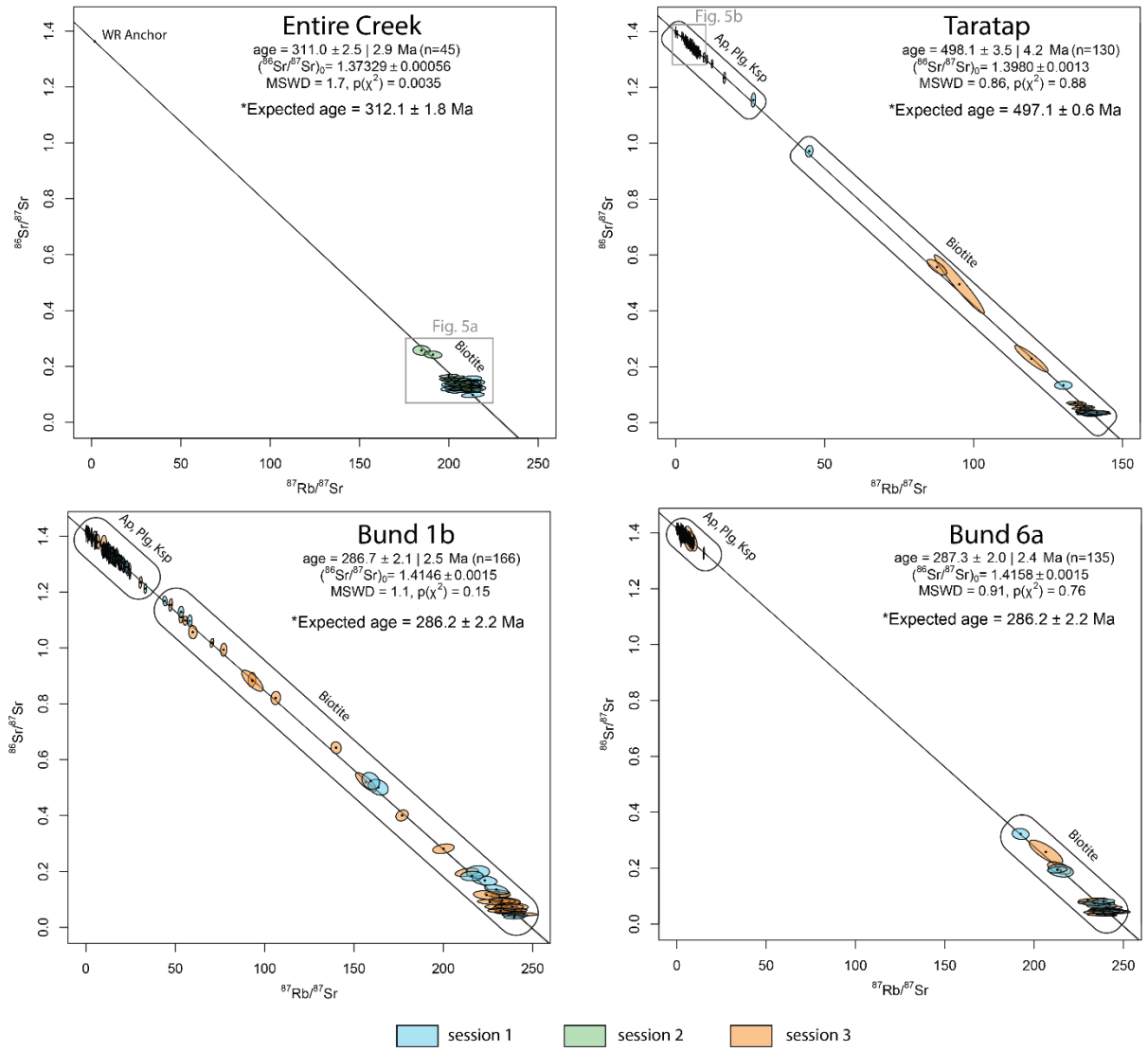

507

508 **Figure 3:** Pooled multi-mineral Rb–Sr isochron dates for the Entire Creek, Taratap and the two
509 Bundarra samples (Bund 1b and Bund 6a). The data were calibrated against NIST-610 as PRM
510 and MDC as MCRM (see text for details). The colour-code refers to the analytical session in which
511 the data was obtained. Biotite analyses plot towards the radiogenic lower-intercept of the inverse
512 isochrons, while feldspar and apatite anchor Rb/Sr ratios plot towards the low-radiogenic end of
513 the isochron regression. All plots were calculated in IsoplotR (Vermeesch, 2018), reporting 95%
514 confidence interval uncertainties (including the uncertainty on the decay-constant) with and
515 without propagated uncertainty from the MDC MCRM. Expected ages are the recalculated Rb–Sr

age from Mortimer et al. (1987) with the Villa et al. (2015) decay constant for the Entire Creek sample; the zircon U-Pb ID-TIMS age reported in Glorie et al. (2023) for the Taratap sample, and the Zircon SHRIMP U-Pb age from Black (2007) for the Bundarra samples (see text for further details).

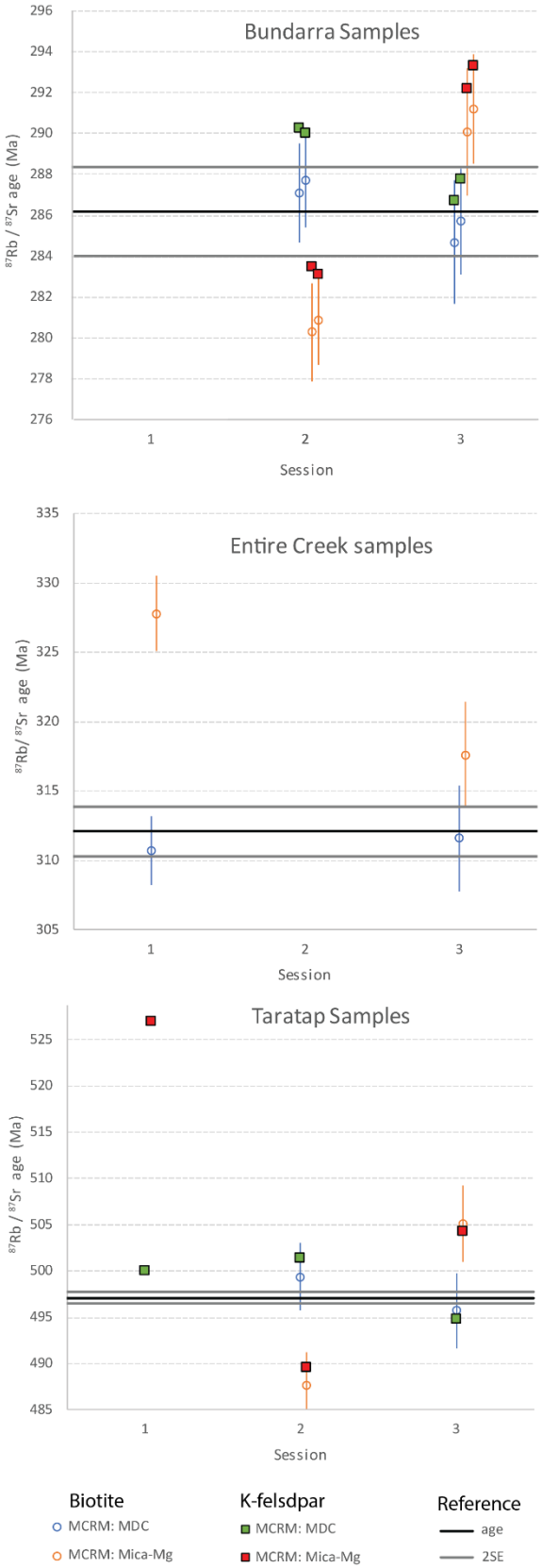
Bundarra Samples
$^{87}Rb / ^{87}Sr$ age (Ma)
296
294
292
290
288
286
284
282
280
278
276
1
2
3
Session
Entire Creek samples
$^{87}Rb/ ^{87}Sr$ age (Ma)
335
330
325
320
315
310
305
1
2
3
Session
Taratap Samples
$^{87}Rb / ^{87}Sr$ age (Ma)
525
520
515
510
505
500
495
490
485
1
2
3
Session
Biotite
MCRM: MDC
MCRM: Mica-Mg
K-felsdpar
MCRM: MDC
MCRM: Mica-Mg
Reference
age
2SE

521

Figure 4: Comparisons of Rb–Sr dates over three analytical sessions, calibrated to either MDC or Mica-Mg as MCRM, with respect to the expected ages for each sample (black line with gray 2SE uncertainty bars). In all cases, NIST-610 was used as PRM. Biotite data are plotted as open circles (blue = calibrated to MDC as MCRM, orange = calibrated to Mica-Mg as MCRM). K-feldspar data are plotted as filled squares (green = calibrated to MDC as MCRM, red = calibrated to Mica-Mg as MCRM).

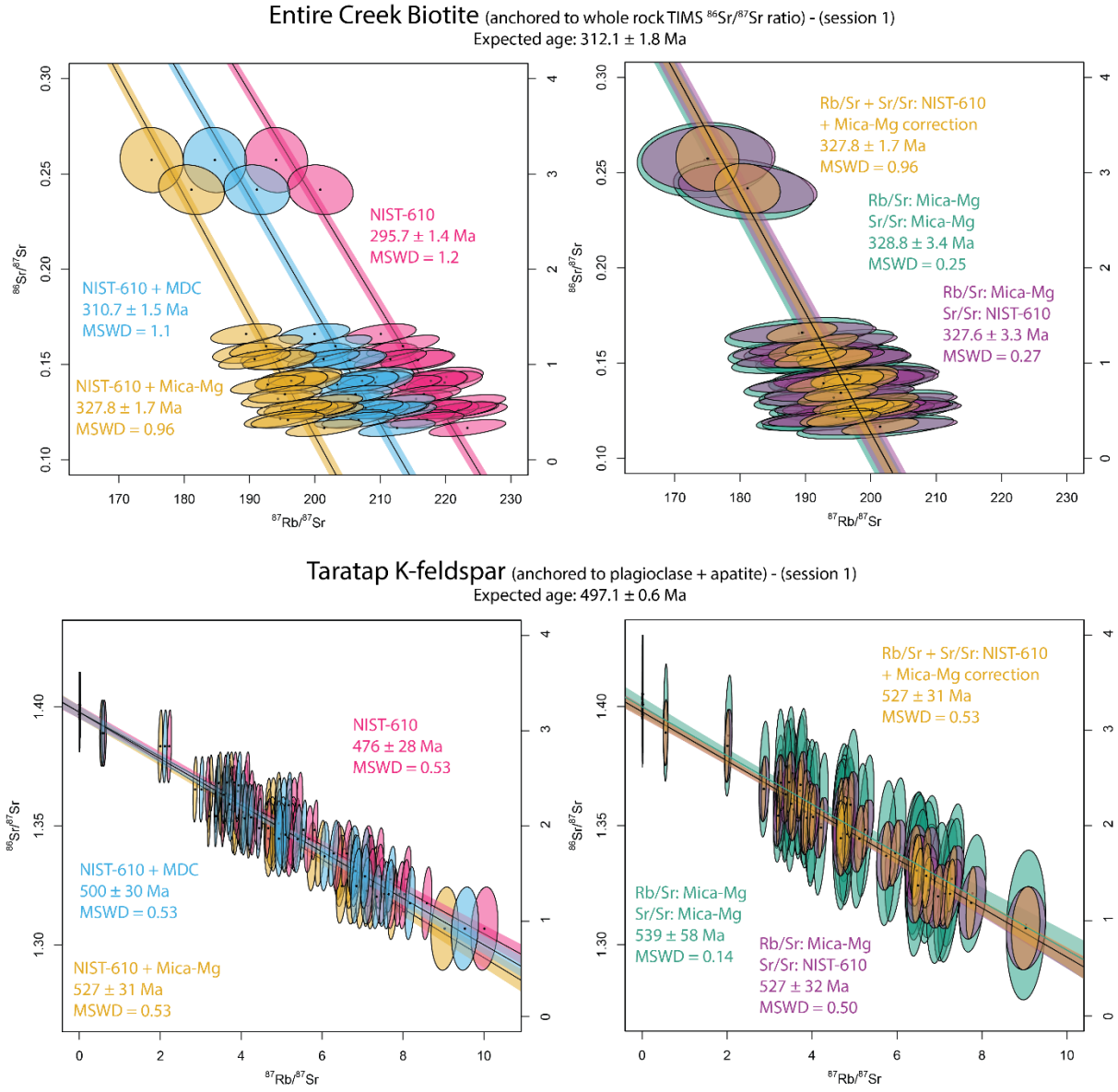

Figure 5: Comparisons of isochron dates obtained using the 4 different calibration protocols using the session 1 biotite Rb–Sr data from the Entire Creek sample and K-feldspar Rb–Sr data from the Taratap sample. Data plotted in red = NIST-610 as PRM without correction for matrix-induced fractionation. Data plotted in green = NIST-610 as PRM with Mica-Mg as MCRM. Data plotted in yellow = NIST-610 as PRM with MDC as MCRM. Data plotted in purple = NIST-610 as PRM for Sr/Sr ratios and Mica-Mg as PRM for Rb/Sr ratios. Data plotted in blue = both Rb/Sr and Sr/Sr ratios calibrated to Mica-Mg as PRM. The biotite data are highly radiogenic and show significant age differences depending on the used MCRM. The K-feldspar data are low radiogenic, resulting in larger and overlapping uncertainties (refer to Figure 3 for full isochron plots). Using NIST-610 as PRM produces the smallest uncertainties on individual data points.

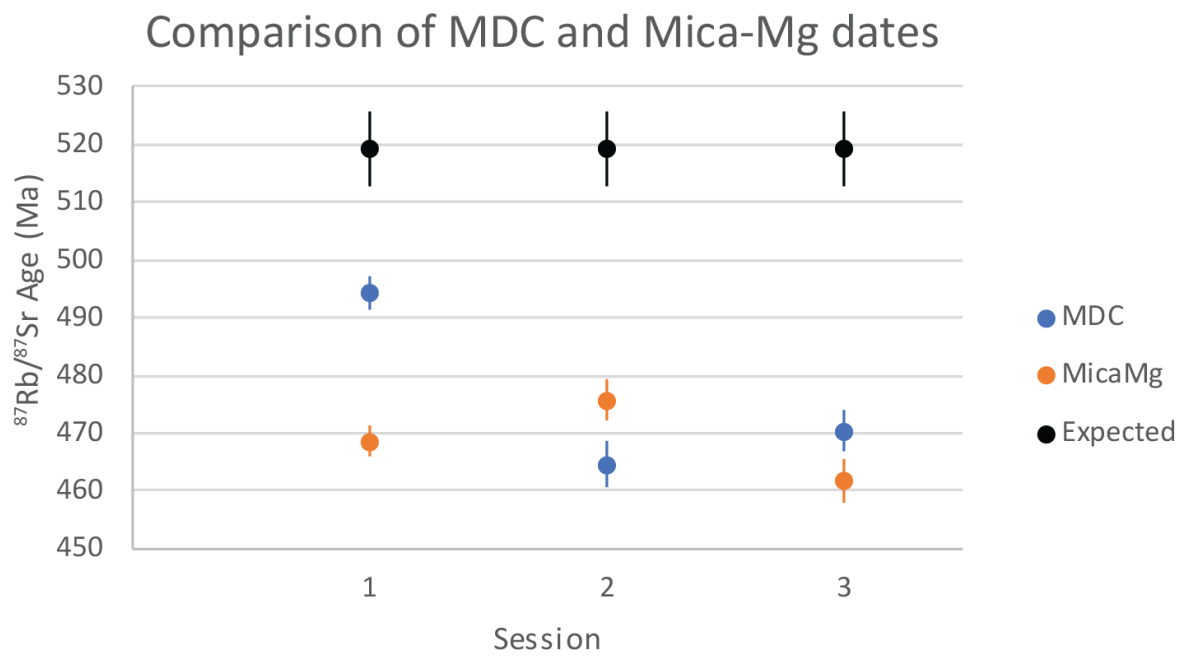

Figure 6: Rb–Sr dates for MDC and Mica-Mg calibrated to NIST-610 over the three analytical sessions used in this paper. The off-set of the Rb–Sr age with respect to the reference age is used to calculate the correction factor on the Rb/Sr ratios. Uncertainties are 2SE.

Figure 7: Long-term (2.5 years) Rb–Sr age data for Mica-Mg and MDC for the lab (Adelaide Microscopy). All uncertainties are 2SE. The top plot shows absolute dates and the bottom plot shows the percentage difference between the MDC and Mica-Mg dates. All data were processed

in the same way using NIST-610 as PRM. The three analytical sessions previously discussed are highlighted by black rims and capture the most extreme differences obtained in our lab to date. Given that MDC as MCRM produces consistently accurate data, the plot indicates that Mica-Mg as PRM can lead to up to 5% inaccuracy in Rb–Sr age calculations.

References

Balcaen, L., Bolea-Fernandez, E., Resano, M., Vanhaecke, F., 2015. Inductively coupled plasma – Tandem mass spectrometry (ICP-MS/MS): A powerful and universal tool for the interference-free determination of (ultra)trace elements – A tutorial review. Analytica Chimica Acta, 894: 7-19.

Black, L., 2007. SHRIMP U–Pb zircon ages obtained during 2006/07 for NSW Geological Survey projects.

Burtt, A.C., Abbot, P.J., 1998. The Taratap Granodioritite, South-East South Australia. MESA Journal, 10: 35-39.

Flood, R.H., Shaw, S.E., 1975. A cordierite-bearing granite suite from the New England Batholith, N.S.W., Australia. Contributions to Mineralogy and Petrology, 52(3): 157-164.

Flood, R.H., Shaw, S.E., 1977. Two "S-type" granite suites with low initial 87Sr/86Sr ratios from the New England Batholith, Australia. Contributions to Mineralogy and Petrology, 61(2): 163-173.

Glorie, S. et al., 2023. Robust laser ablation Lu-Hf dating of apatite: an empirical evaluation. Geological Society of London Special Publication, In press.

Gorojovsky, L., Alard, O., 2020. Optimisation of laser and mass spectrometer parameters for thein situanalysis of Rb/Sr ratios by LA-ICP-MS/MS. JOURNAL OF ANALYTICAL ATOMIC SPECTROMETRY, 35(10): 2322-2336.

Hogmalm, K.J., Zack, T., Karlsson, A.K.O., Sjoqvist, A.S.L., Garbe-Schonberg, D., 2017. In situ Rb-Sr and K-Ca dating by LA-ICP-MS/MS: an evaluation of N2O and SF6 as reaction gases. Journal of Analytical Atomic Spectrometry, 32(2): 305-313.

Jackson, S.E., Günther, D., 2003. The nature and sources of laser induced isotopic fractionation in laser ablation-multicollector-inductively coupled plasma-mass spectrometry. Journal of Analytical Atomic Spectrometry, 18(3): 205-212.

Jegal, Y. et al., 2022. Characterisation of Reference Materials for In Situ Rb-Sr Dating by LA-ICP-MS/MS. Geostandards and Geoanalytical Research, 46(4): 645-671.

Jeon, H., Williams, I.S., Chappell, B.W., 2012. Magma to mud to magma: Rapid crustal recycling by Permian granite magmatism near the eastern Gondwana margin. Earth and Planetary Science Letters, 319-320: 104-117.

Kirkland, C.L. et al., 2023. Dating mylonitic overprinting of ancient rocks. Communications Earth & Environment, 4(1): 47.

Košler, J. et al., 2005. Chemical and phase composition of particles produced by laser ablation of silicate glass and zircon—implications for elemental fractionation during ICP-MS analysis. Journal of Analytical Atomic Spectrometry, 20(5): 402-409.

Larson, K.P., Button, M., Shrestha, S., Camacho, A., 2023. A comparison of 87Rb/87Sr and 40Ar/39Ar dates: Evaluating the problem of excess 40Ar in Himalayan mica. Earth and Planetary Science Letters, 609: 118058.

Laureijs, C.T., Coogan, L.A., Spence, J., 2021. In-situ Rb-Sr dating of celadonite from altered upper oceanic crust using laser ablation ICP-MS/MS. Chemical Geology, 579.
Li, S.-S. et al., 2020. Coupled U-Pb and Rb-Sr laser ablation geochronology trace Archean to Proterozoic crustal evolution in the Dharwar Craton, India. Precambrian Research, 343: 105709.
Li, Y., Vermeesch, P., 2021. Short communication: Inverse isochron regression for Re–Os, K–Ca and other chronometers. Geochronology, 3(2): 415-420.
Liebmann, J., Kirkland, C.L., Kelsey, D.E., Korhonen, F.J., Rankenburg, K., 2022. Lithological fabric as a proxy for Rb-Sr isotopic complexity. Chemical Geology, 608.
Longerich, H.P., Günther, D., Jackson, S.E., 1996. Elemental fractionation in laser ablation inductively coupled plasma mass spectrometry. Fresenius' Journal of Analytical Chemistry, 355(5): 538-542.
Moens, L.J., Vanhaecke, F.F., Bandura, D.R., Baranov, V.I., Tanner, S.D., 2001. Elimination of isobaric interferences in ICP-MS, using ion–molecule reaction chemistry: Rb/Sr age determination of magmatic rocks, a case study. Journal of Analytical Atomic Spectrometry, 16(9): 991-994.
Mortimer, G.E., Cooper, J.A., James, P.R., 1987. U Pb and Rb Sr geochronology and geological evolution of the Harts Range ruby mine area of the Arunta Inlier, central Australia. Lithos, 20(6): 445-467.
Norris, A., Danyushevsky, L., 2018. Towards Estimating the Complete Uncertainty Budget of Quantified Results Measured By LA-ICP-MS. Goldschmidt, Boston, USA (2018).
Olierook, H.K.H. et al., 2020. Resolving multiple geological events using in situ Rb–Sr geochronology: implications for metallogenesis at Tropicana, Western Australia. Geochronology, 2(2): 283-303.
Phillips, G., Landenberger, B., Belousova, E.A., 2011. Building the New England Batholith, eastern Australia—Linking granite petrogenesis with geodynamic setting using Hf isotopes in zircon. Lithos, 122(1): 1-12.
Redaa, A. et al., 2023. Testing Nano-Powder and Fused-Glass Mineral Reference Materials for In Situ Rb-Sr Dating of Glauconite, Phlogopite, Biotite and Feldspar via LA-ICP-MS/MS. Geostandards and Geoanalytical Research, 47(1): 23-48.
Redaa, A. et al., 2021. Assessment of elemental fractionation and matrix effects during in situ Rb-Sr dating of phlogopite by LA-ICP-MS/MS: implications for the accuracy and precision of mineral ages. Journal of Analytical Atomic Spectrometry, 36(2): 322-344.
Roberts, N.M.W. et al., 2017. A calcite reference material for LA-ICP-MS U-Pb geochronology. Geochemistry, Geophysics, Geosystems, 18(7): 2807-2814.
Rosel, D., Zack, T., 2022. LA-ICP-MS/MS Single-Spot Rb-Sr Dating. Geostandards and Geoanalytical Research, 46(2): 143-168.
Rosenbaum, G., Li, P., Rubatto, D., 2012. The contorted New England Orogen (eastern Australia): New evidence from U-Pb geochronology of early Permian granitoids. Tectonics, 31(1).
Sengun, F., Erlandsson, V.B., Hogmalm, J., Zack, T., 2019. In situ Rb-Sr dating of K-bearing minerals from the orogenic Akcaabat gold deposit in the Menderes Massif, Western Anatolia, Turkey. JOURNAL OF ASIAN EARTH SCIENCES, 185.
Shaw, S.E., Flood, R.H., 1981. The New England Batholith, eastern Australia: Geochemical variations in time and space. Journal of Geophysical Research: Solid Earth, 86(B11): 10530-10544.
Simpson, A. et al., 2022. In situ Lu–Hf geochronology of calcite. Geochronology, 4(1): 353-372.
Tillberg, M. et al., 2021. Reconstructing craton-scale tectonic events via in situ Rb-Sr geochronology of poly-phased vein mineralization. Terra Nova, 33(5): 502-510.
Tillberg, M. et al., 2020. In situ Rb-Sr dating of slickenfibres in deep crystalline basement faults. Scientific Reports, 10(1).
Vermeesch, P., 2018. IsoplotR: A free and open toolbox for geochronology. Geoscience Frontiers, 9(5): 1479-1493.

637 Villa, I.M., De Bièvre, P., Holden, N.E., Renne, P.R., 2015. IUPAC-IUGS recommendation on the half life of
638 87Rb. Geochimica et Cosmochimica Acta, 164: 382-385.
639 Wang, C.Y. et al., 2022. Advances in in-situ Rb-Sr dating using LA-ICP-MS/MS: applications to igneous rocks
640 of all ages and to the identification of unrecognized metamorphic events. Chemical Geology, 610.
641 Woodhead, J.D., Hergt, J.M., 2001. Strontium, Neodymium and Lead Isotope Analyses of NIST Glass
642 Certified Reference Materials: SRM 610, 612, 614. Geostandards Newsletter, 25(2-3): 261-266.
643 Zack, T., Hogmalm, K.J., 2016. Laser ablation Rb/Sr dating by online chemical separation of Rb and Sr in an
644 oxygen-filled reaction cell. Chemical Geology, 437: 120-133.